Iran J Nucl Med. 2024;32(2):183-193 [Serial No. 63]

Homepage: https://irjnm.tums.ac.ir/

ORIGINAL RESEARCH ARTICLE

Standardization and optimization of Siemens Biograph TruePoint PET/CT acquisition and reconstruction parameters: Simultaneous qualitative and quantitative assessments

Habibeh Vosoughi[1,2], Farshad Emami[3], Mehdi Momennezhad[4], Parham Geramifar[2], Arman Rahmim[5]

[1]*Department of Medical Physics, Mashhad University of Medical Science, Mashhad, Iran*

[2]*Research Center for Nuclear Medicine, Tehran University of Medical Science, Tehran, Iran*

[3]*Nuclear Medicine and Molecular Imaging Department, Imam Reza International University, Razavi Hospital, Mashhad, Iran*

[4]*Nuclear Medicine Research Center, Faculty of Medicine, Mashhad University of Medical Sciences, Mashhad, Iran*

[5]*Departments of Radiology and Physics, University of British Columbia, Vancouver, Canada*

ARTICLE INFO

Article History:
Received: 22 October 2023
Revised: 29 April 2024
Accepted: 05 May 2024
Published Online: 04 June 2024

Keyword:
PET/CT
Standardization
Optimization
Image quality

*Corresponding Author:
Dr. Parham Geramifar
Address: Research Center for Nuclear Medicine, Shariati Hospital, North Kargar Ave. 1411713135, Tehran, Iran
Email: pgeramifar@tums.ac.ir

ABSTRACT

Introduction: Data acquisition and image reconstruction protocols affect image quality and quantification accuracy in PET imaging. We aimed to standardize and optimize image acquisition, and reconstruction parameter sets using a simultaneous quantitative and qualitative assessment framework for a lutetium oxyorthosilicate (LSO)-based PET/CT scanner.

Methods: The NEMA IEC Body Phantom acquisition was performed in list mode for 10 minutes with four spheres to background ratios (SBRs). Raw PET data were reconstructed using 60 different protocols. Image quality was evaluated for standardization using contrast, CNR, and noise. Recovery coefficient (RC) measurements were performed for different common VOI definitions.

Results: No significant differences were observed between RCs for various acquisition durations. The contrast to noise ratio (CNR) increased at all SBRs by expanding the acquisition duration from 60 to 600 seconds. PET scan time was reduced to 90 seconds per bed position while preserving image quality. Up to 50% improvement in CNR for the highest sub-iteration with a high level of smoothing was observed. PSF-based reconstruction produced a positive bias of RC_{max} in high SBRs (8 and 10) using higher sub-iterations (30 to 60) with Gaussian filters less than 6 mm FWHM. Moreover, a Sub-iteration of more than 32 with a 4-6 mm FWHM Gaussian filter provides optimized reconstruction sets.

Conclusion: Our study demonstrates it would be feasible for PET image acquisition and reconstruction settings to simultaneously allow optimal lesion detection with high image quality while providing accurate quantification.

Use your device to scan and read the article online

How to cite this article: Vosoughi H, Emami F, Momennezhad M, Geramifar P, Rahmim A. Standardization and optimization of Siemens Biograph TruePoint PET/CT acquisition and reconstruction parameters: Simultaneous qualitative and quantitative assessments**.** Iran J Nucl Med. 2024;32(2):183-193.

https://doi.org/10.22034/IRJNM.2024.129432.1579

INTRODUCTION

PET/CT images are used extensively for diagnosis, staging, restaging, response to treatment, as well as detection of tumor recurrence using quantitative and semi-quantitative analysis [1]. While visual evaluation of PET/CT images is a powerful diagnostic method, additional use of the standard uptake value (SUV) as a semi-quantitative metric for assessment of PET/CT images is a valuable and popular adjunct to visual inspection [2, 3]. Though prone to many sources of variation and errors, the semi-quantitative method using SUV is currently used in clinical practice. Minimizing variability of SUV is achieved by standardization of scanner calibration, patient preparation, image acquisition, and reconstruction protocols, recommended by different organizations such as the European Association of Nuclear Medicine (EANM) [1, 4], Society of Nuclear Medicine and Molecular Imaging (SNMMI) [5] and Uniform Protocols for Imaging in Clinical Trials (UPICT) [6]. Acquisition parameters such as injected activity and time per bed position are affected by scanner hardware characteristics, so they should be standardized and optimized. Differences in image reconstruction methods using advanced algorithms such as resolution recovery and time of flight make standardization and generalization difficult [3].

Although advanced reconstruction algorithms such as PSF or with the combination of time of flight (PSF+TOF) improve lesion detectability and image quality, they also significantly affect SUV calculation [7]. The significance of SUV accuracy makes the optimization of protocols crucial [8]. Therefore, acquisition and reconstruction protocols should be optimized to achieve good qualitative and quantitative accuracy in the shortest possible scan time. The current study aims to propose an organized framework to find an optimized protocol that simultaneously reduces quantitative variability in the intra-scanner investigation, with optimized acquisition duration, equipped with image reconstruction sets that allow optimal lesion detectability, high image quality, and accurate quantitative metrics.

METHODS

Phantom preparation

NEMA IEC Body Phantom Set™ contains six fillable spheres with various diameters of 10, 13, 17, 22, 28, 37 mm and a total volume of 9.7 liters was used. The Phantom was filled with a homogenized solution of 2-deoxy-2-[^{18}F]fluoro-D-glucose ([^{18}F]FDG) with an activity concentration of 3.5kBq/ml as background. Spheres were then filled with [^{18}F]FDG solution to achieve sphere to background ratios (SBR) of 4, 6, 8, and 10 to simulate different tumor presentations [9].

Acquisition and reconstruction setup

Data acquisitions of the Phantom were performed for 10 minutes in list mode on the Biograph6 TrueV PET/CT scanner (Siemens Healthcare, Erlangen, Germany) with a 6-slice spiral CT component. PET images were reconstructed in varying acquisition duration, six different sub-iterations 16, 28, 32, 42, 56, 63, and five Gaussian post-smoothing filters with FWHM values of 2, 4, 6, 8, and 10mm. OSEM reconstruction algorithm or PSF modeling using TrueX (Syngo software, Siemens medical solutions) was applied for each reconstruction set. Normalization, Attenuation, Scatter, and Decay corrections were applied for all reconstructions. The reconstructed matrix size was 168×168 resulting in a 4.07×4.07×2.027mm voxel size. All data analysis including VOI delineation and quantification was performed using the Syngo MMWP software (Siemens healthcare, Erlangen, Germany).

Data analysis

Image quality parameters

The present study assessed image quality using three indices: contrast, contrast to noise ratio (CNR), and coefficient of variation (CV). Contrast and CNR are calculated as follows:

$$\text{Contrast} = {\text{Cmax(sphere)}}\Big/{\text{Cmean(background)}} \quad (1)$$

$$\text{CNR} = \frac{\text{Cmean(sphere)} - \text{Cmean(background)}}{\text{SD (background)}} \quad (2)$$

Where C_{mean}(sphere) and C_{mean}(background) denote the mean count value of ROIs drawn in the sphere and background, respectively, C_{max}(sphere) is the maximum count value of the sphere, and SD denotes the standard deviation of the background.

The CV percentage describes ensemble or statistical noise in the image, which influences detectability and image quality. And it is calculated as follows:

$$\text{CV}(\%) = \frac{\text{SD(background)}}{\text{Cmean(background)}} * 100 \quad (3)$$

A trans-axial slice with the best visualization of all spheres was used to draw the volume of interest (VOI) for spheres and 12 sets of VOIs in

the background; each contains six VOIs with diameters identical to the spheres.

Quantitative indices

The recovery coefficient (RC) was calculated as the measured to true activity concentration ratio. For each reconstruction, 3D-50% isocontour VOI was drawn fitted to the spheres, then maximum and mean voxel values were used to calculate RC_{max} and $RC_{50\%}$, respectively. RC_{peak} was measured as the average voxels of spherical VOI with 1 cm^3 volume placed in the highest uptake region [10].

Scan time optimization

For time optimization, the effects of different acquisition duration on CNR in 10mm and 13mm spheres (the most difficult ones to detect), on CV% for spherical VOI (diameter of 10 and 37mm), and RC_{max}, $RC_{50\%}$, and RC_{peak} for all sphere sizes were studied. The PET list-mode data of four SBRs were reconstructed based on the routine image reconstruction protocol (PSF-based reconstruction with 42 sub-iterations and 3mm FWHM Gaussian filter), mimicking the acquisition duration of 60 to 600 seconds.

Assessment of image noise based on the CV% index was performed by statistical analysis for all SBRs. Wilcoxon signed-rank test was used considering the non-parametric distribution of CV% data. The significance level was set at 0.05. To evaluate detectability and image quality, the CNR of two spheres with the smallest sizes (10 and 13mm diameters) was calculated to imitate small lesions with variable uptake in clinical scenarios with different acquisition duration per bed position. Each SBR was also investigated separately. The percentage differences (D%) in CNRs for all SBRs between two selected sizes and between consecutive time intervals were measured as follows:

$$D\% = \frac{|CNR(t1)-CNR(t2)|}{CNR(t1)+CNR(t2)} * 100 \quad (4)$$

Differences in RC_{max}, $RC_{50\%}$, and RC_{peak} between different time intervals per bed position (60, 90, 120, 150, 180, 300, and 600seconds) were evaluated using paired t-test. Also, the RCs for different acquisition duration were compared with a 600sec reference time. The percentage changes of RC_{max}, $RC_{50\%}$, and RC_{peak} were calculated using:

$$\Delta RC = \frac{RC(t)-RC(t.reference)}{RC(t.reference)} * 100 \quad (5)$$

Finally, the root mean square error (RMSE) was used to evaluate the accuracy of RC values in various acquisition durations with changes in the sphere size. The RMSE was calculated using:

$$RMSE = \sqrt{\frac{1}{6}\sum_{d=10,13,17,22,28,37mm}(RC_d - 1)^2} \quad (6)$$

Optimized reconstruction parameters regarding image quality

Using the optimized time, parameters influencing the image quality, including SBR, size of object, reconstruction algorithm (with/without PSF correction), number of sub-iterations, and FWHM of Gaussian filter, were investigated. Different reconstruction sets were evaluated by measuring the CNR, contrast, and CV% for different sphere sizes and SBRs.

Two nuclear medicine physicians performed a visual assessment for the overall quality and detectability of the smallest sphere in different SBRs. In the case of disagreement between them, the interpretation of the third nuclear medicine physician was accepted. Overall image quality was categorized into four grade scales from 1 to 4 (1: not visible, 2: poor, 3: good, 4: excellent).

PET image quantification

Considering the importance of quantification, reconstruction sets in different sphere sizes and SBRs should also be evaluated for accurate quantification. Regardless of object size, the optimal RC value should ideally be around unity (1±0.1). However, inaccurate results were produced in the presence of small objects (d<15mm) [11], where partial volume effects (PVE) are most pronounced.

The optimized reconstruction setup was determined in three steps. First, the effect of sub-iterations without filtering in one sphere size was evaluated. The RCs were plotted for spheres with a diameter of 17mm versus sub-iteration. Second, a suitable sub-iteration was selected, and the effect of the Gaussian post-smoothing filter on the 17mm sphere size was assessed. Finally, the RCs, as a function of sphere size, were plotted using the reconstruction method, as described in the two previous steps, with or without the resolution recovery algorithm. Based on these results, optimal reconstruction sets were sought to achieve maximum RC, approaching unity.

RESULTS

Scan time optimization

The CNR, contrast, and CV% were plotted against the acquisition duration to assess the effect of acquisition duration on image quality. Figure 1 shows variations in contrast and CNR in different scan times for two sphere sizes (10 and 22mm). Longer acquisition duration resulted in an increase in the CNR and a significant noise reduction. The CNR showed an almost two-fold

increase at SBR 4 and 6 and a 1.5-fold increase at SBR 8 and 10 by expanding the acquisition duration from 60 to 600 seconds in all sphere sizes. The contrast slightly increased at SBRs of 8 and 10, while it negligibly reduced at SBR4 and 6; overall, it was constant over time. Besides, increasing the size of spherical VOI in the background led to a 3% increase in noise. Although in some image reconstruction settings with a high number of sub-iterations and low FWHM of the Gaussian filter, the CV% was higher than the EARL threshold (15%) [4], it was lower than the EARL threshold when the acquisition duration was 180seconds or longer.

Expectedly, increasing the acquisition duration influenced image noise by reducing the CV%. The results revealed that acquisition duration longer than 90 seconds was not associated with a significant difference in the CV% compared to other acquisition duration (Table 1).

The results of the CNR assessment are presented in detail in Table 2. A significant difference was found in the CNR between 30 and 60 seconds of acquisition duration compared to other intervals. The percentage difference significantly changed between 150 and 180seconds at SBR4. The percentage difference of CNR was insignificant in acquisition duration longer than 180 seconds. Based on the findings, the detectability performance or CNR of the smallest sphere at a low activity concentration was more than five at acquisition duration of 60 seconds or longer. The CNR of the 10mm sphere ranged from 3 to 8.9 for an acquisition duration of 30 to 600seconds. According to Figure 2, the trans-axial images of the NEMA phantom at SBR 4 in various acquisition durations per bed position showed that the smallest sphere was detectable, even in short acquisition duration (60 seconds). No significant difference was observed in the RC_{max}, $RC_{50\%}$, or RC_{peak}, regardless of the acquisition duration (p-values: 0.07-0.99). ΔRC was less than 5% at an acquisition duration longer than 90 seconds for all spheres except the smallest one (d=10mm). However, the ΔRC was less than 5% after 180 seconds in 10 mm spheres. The results are presented in detail in Table 3.

The RMSE value for the routine clinical reconstruction set in all SBRs was in the ranges of 27.31-29.62%, 25.27-27.33%, and 12.71-13.44% for RC_{max}, $RC_{50\%}$, and RC_{peak}, respectively, in acquisition duration of 60 to 600 seconds (Table 4). Overall, increasing the scan time did not significantly affect the accuracy of PET image quantitation. Of all quantitative metrics, the RC_{peak} is the most accurate parameter.

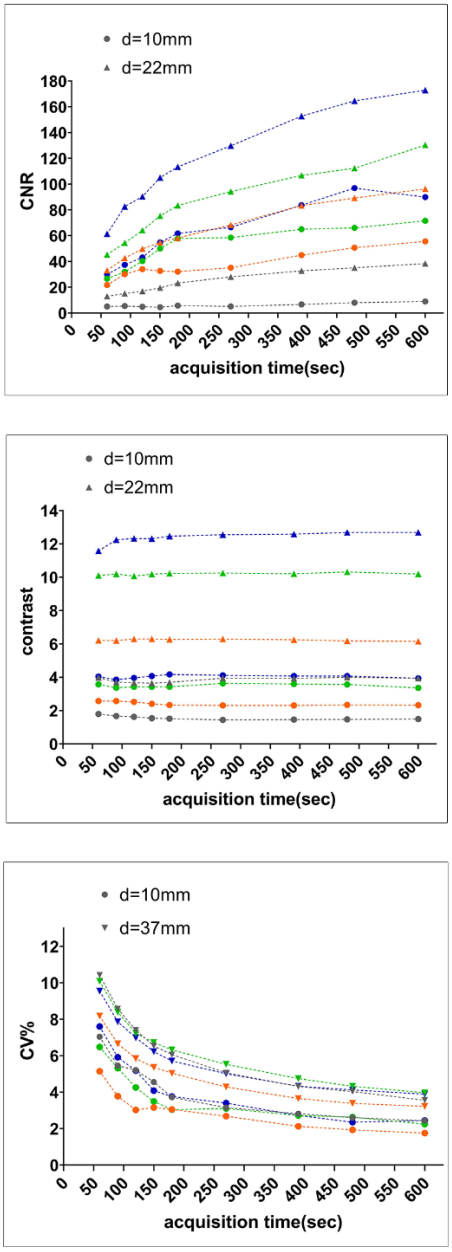

Figure 1. CNR, contrast, and CV% against acquisition duration in resolution recovery reconstruction, Sub-iteration 42 with 3 mm FWHM of Gaussian filter (blue = SBR10, green = SBR8, orange = SBR6, gray = SBR4)

Table 1. Comparison of coefficient of variations (CVs) between pairs of acquisition duration

Difference between two time point	p-value
30sec vs. 60sec	0.02*
60sec vs. 90sec	0.04*
90sec vs.120sec	0.12
120sec vs. 150sec	0.15
150sec vs. 180sec	0.33
210sec vs. 240sec	0.45
240sec vs. 270sec	0.49
270sec vs. 300sec	0.57

* shows a difference with p-value < 0.05

Table 2. Percentage difference (D%) in contrast to noise ratio (CNR) values between acquisition duration for different spheres to background ratios (SBRs). The two smallest spheres of the NEMA phantom were assessed to find optimized scan time. D% values found to be higher than 10% are shown in bold. A significant difference was found in the CNR between 30 and 60 seconds of acquisition duration compared to other intervals. The percentage difference significantly changed between 150 and 180seconds at SBR4

Spheres to background ratio (SBR) D% between acquisition duration	4		6		8		10	
	d=10	d=13	d=10	d=13	d=10	d=13	d=10	d=13
30sec vs. 60sec	**25.22**	**72.90**	**22.69**	**52.74**	**28.62**	**29.91**	**65.64**	**61.43**
60sec vs. 90sec	3.10	5.42	**16.24**	**10.43**	9.07	**13.10**	**11.10**	9.85
90sec vs. 120sec	4.60	2.81	**10.21**	**10.59**	**11.52**	9.11	7.04	3.27
120sec vs. 150sec	4.04	8.79	6.36	0.11	9.76	8.67	**11.96**	**10.56**
150sec vs. 180sec	**12.06**	**11.88**	0.79	2.50	7.23	6.87	5.89	3.59
180sec vs. 210sec	2.98	2.09	4.81	8.22	4.48	2.72	1.84	5.68
210sec vs. 240sec	1.71	3.05	2.12	2.78	2.32	2.45	2.26	2.92
240sec vs. 270sec	3.1	0.26	6.47	1.78	2.74	1.87	0.33	0.03
270sec vs. 300sec	4.21	4.43	6.92	6.12	1.12	1.97	5.72	4.56
300sec vs. 360sec	7.76	3.60	5.32	6.80	5.95	6.05	7.59	7.07
360sec vs. 420sec	5.72	2.87	2.19	2.68	2.26	2.40	4.60	5.41
420sec vs. 480sec	5.69	3.85	5.32	4.27	0.35	2.27	9.40	7.15
480sec vs. 540sec	2.62	0.50	0.75	7.81	7.79	8.95	5.02	3.61
540sec vs. 600sec	3.10	3.71	4.29	8.08	0.44	6.14	2.28	1.43

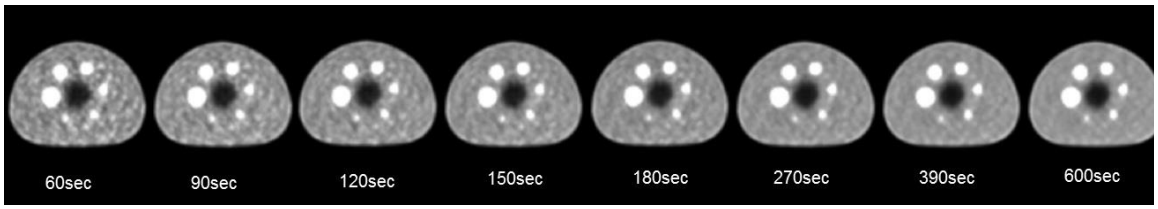

Figure 2. Effect of acquisition duration on image quality. A trans-axial image of the NEMA phantom with SBR4 is shown. Increasing frame duration reduces image noise and improves CNR and contrast

Table 3. Means of ΔRC in all SBRs compared to reference RC at 600 sec

		60 vs. 600s	90 vs. 600s	120 vs. 600s	150 vs. 600s	180 vs. 600s	300 vs. 600s
d=10mm	RC_{max}	13	8.2	7.3	4.5	2.4	5
	$RC_{50\%}$	9.1	9.4	7.5	7	4	1
	RC_{peak}	12.5	8	6	7.5	5	5
d=13mm	RC_{max}	4.7	2.3	2.7	2.2	1.5	3.6
	$RC_{50\%}$	4.8	4.8	4.9	3.4	2.5	4.2
	RC_{peak}	4.6	1.7	2	1.5	1.5	1.5
d=17mm	RC_{max}	5.6	4	3	2.7	2.7	2
	$RC_{50\%}$	4.5	4.4	3	3	2.7	1.2
	RC_{peak}	4.5	2	3	3	2.5	1.2
d=22mm	RC_{max}	3.5	2	2	2.5	2	2
	$RC_{50\%}$	3	2.3	3	2.5	2.3	2
	RC_{peak}	5	2.5	3	1.5	2.2	1
d=28mm	RC_{max}	5	3.5	1	2.4	2	2
	$RC_{50\%}$	3.5	2.2	1.5	2.5	2	1.5
	RC_{peak}	4.4	2.3	1.5	2	2.2	3
d=37mm	RC_{max}	5	2	2.5	2.5	3	2.6
	$RC_{50\%}$	2.5	1	1.6	1.8	1.7	1.3
	RC_{peak}	2.5	1.5	2	1.5	2	2

RC: Recovery coefficient; SBRs: Spheres to background ratio

Table 4. RMSE values for RC_{max}, $RC_{50\%}$ and RC_{peak} indifferent acquisition duration and SBRs

		60sec	90sec	120sec	180sec	300sec	600sec
SBR 4	RC_{max}	27.86%	29.15%	30.33%	32.06%	32.07%	31.45%
	$RC_{50\%}$	28.87%	26.29%	25.91%	25.58%	25.26%	24.29%
	RC_{peak}	14.02%	14.03%	14.11%	14.35%	14.57%	14.13%
SBR 6	RC_{max}	27.03%	27.39%	27.68%	29.13%	29.30%	28.79%
	$RC_{50\%}$	27.86%	26.66%	26.67%	26.53%	26.14%	25.61%
	RC_{peak}	12.87%	13.36%	13.63%	13.51%	13.86%	13.77%
SBR 8	RC_{max}	28.74%	28.90%	28.51%	29.24%	27.95%	29.29%
	$RC_{50\%}$	25.89%	25.92%	25.85%	25.69%	25.84%	25.56%
	RC_{peak}	12.03%	12.24%	12.23%	11.82%	12.07%	12.01%
SBR 10	RC_{max}	26.54%	27.79%	27.83%	27.43%	26.40%	27.12%
	$RC_{50\%}$	26.62%	26.70%	25.70%	25.64%	25.78%	25.92%
	RC_{peak}	12.58%	12.15%	12.63%	13.01%	13.10%	12.98%

RMSE: Root mean square error, RC: Recovery coefficient, SBR: Spheres to background ratio

Optimized reconstruction parameter sets regarding image quality

The average CNR, CV%, and contrast of six spheres were plotted as a function of reconstruction parameters using two different algorithms, with or without PSF correction (Figure 3). The two reconstruction algorithms showed similar trends. However, the PSF improved CNR by 2-25% and contrast by 4-7% while reducing noise by about 3-20% compared to the non-PSF algorithm. CNR was increased by more than 50% if the highest sub-iteration number with a high level of smoothing was used (relative to the lowest sub-iteration and smoothing level), whereas CV% and contrast values were reduced by more than 70% and 30%, respectively. As shown in Figure 3, contrast and CV% increased by increasing the number of sub-iterations, while the CNR decreased. An increase in FWHM seems to reduce noise and increase CNR, whereas over-smoothing PET images can degrade contrast. Generally, CNR and contrast have an inverse relationship in reconstruction settings.

The 10mm sphere was used for evaluating lesion detectability, especially at an SBR of 4. The CNR of SBRs higher than 4 was more than 5 (Rose criterion); therefore, the 10mm sphere could be observed. In this study, detectability was defined by CNR, and sharpness was determined by contrast. The trade-off plot between the two metrics, as a function of reconstruction parameters at SBR4, is shown in Figure 4. The width of the Gaussian filter was more important than the number of sub-iterations in the detectability assessment. The contrast was impaired by increasing the FWHM of the Gaussian filter, whereas the CNR was improved. Based on the trade-off between contrast and CNR, the optimal image reconstruction for the best detectability was recommended to be 6mm FWHM Gaussian filters and a higher number of sub-iterations.

Figure 5 presents a visual assessment of the overall image quality and detectability by nuclear medicine specialists. The image reconstruction using PSF correction was appropriate with sub-iterations between 4×8 and 2×21 over a range of SBRs (score 3); for higher SBRs, more sub-iterations were required (score 4).

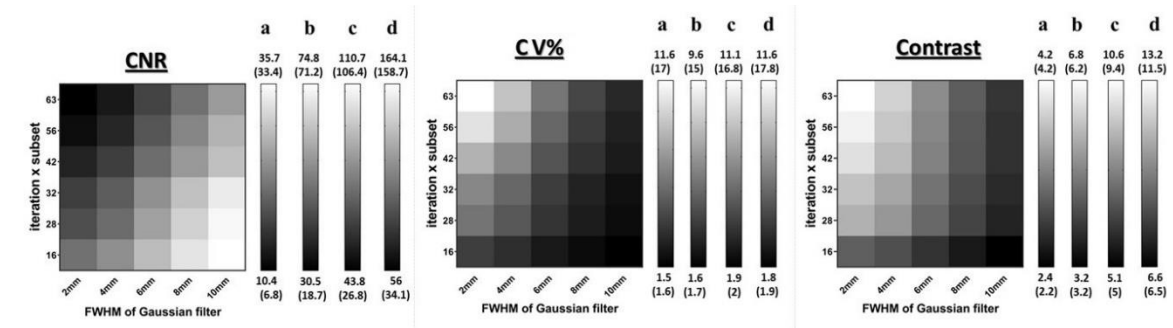

Figure 3. Patterns of grey-level shades demonstrate the effect of sub-iterations (iteration x subsets) and FWHM of Gaussian filter on CNR, contrast, and CV% as quantitative indices of image quality. Each bar represents maximum and minimum corresponding values for means of all spheres for SBR values of (a) 4, (b) 6, (c) 8, and (d) 10, with (without) PSF correction

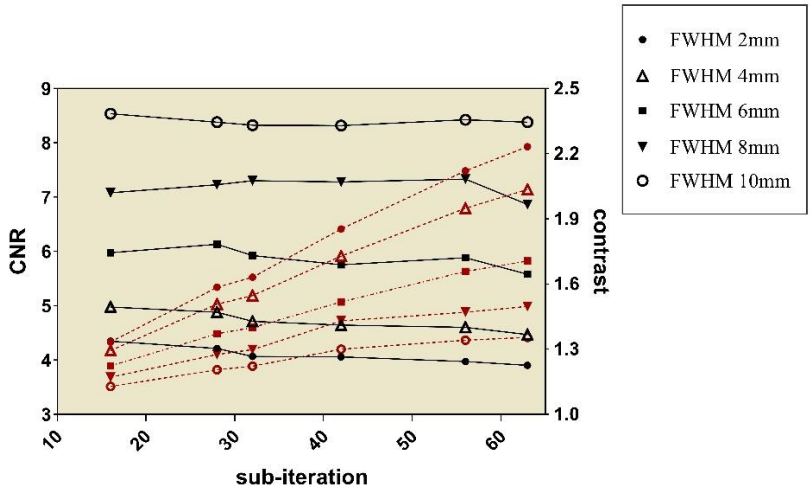

Figure 4. Relationship between CNR and contrast as a function of sub-iteration numbers and FWHM of Gaussian filter using PSF correction algorithm to assess the detectability of 10mm hot sphere in SBR4. Black and red curves represent CNR and contrast, respectively

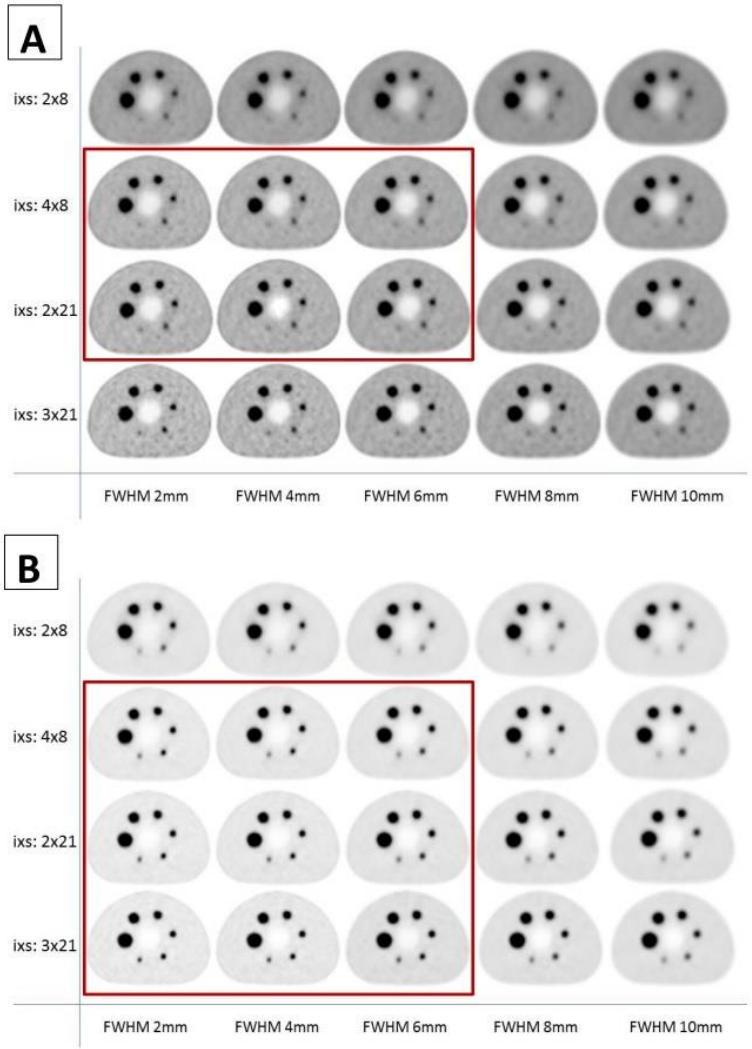

Figure 5. Transverse images of NEMA IEC Body Phantom Set™ reconstructed using various numbers of sub-iteration (i x s) with 5 different FWHMs of Gaussian filter. (A) SBR4 and (B) SBR10. Preferred reconstruction methods by physicians are shown in the red box

Effects of reconstruction parameters in PET image quantification

Figure 6 and Figure 7 show the RC_{max}, $RC_{50\%}$, and RC_{peak} as functions of sub-iteration number, FWHM of Gaussian filter, and sphere size in various SBRs. Each parameter was separately assessed while considering other parameters constant. Figure 6A shows the effects of sub-iteration number on the RCs in 17 mm spheres with no smoothing filter. All RC values increased by increasing the number of sub-iterations. The $RC_{50\%}$ and RC_{peak} approached one with sub-iterations of more than 32 in both algorithms. The RC_{max} showed an overshoot of almost 40% with sub-iterations more than 32 in PSF-based reconstruction due to an edge artifact. Also, this artifact significantly influenced the RC_{max} at higher SBRs (8 and 10). Overall, no edge artifact appeared in the non-PSF algorithm.

According to Figure 6B, the RCs decreased by increasing the FWHM of the Gaussian filter without and with PSF reconstruction algorithms with 32 sub-iterations and a 17mm sphere size. As expected, less filtration led to higher RC values. The upward bias of RC_{max} was reduced using a suitable smoothing filter or measuring RC_{peak} instead of RC_{max}. Besides, the suitable FWHM to obtain accurate RC values and adequate image quality was selected. The use of 4 and 6 mm FWHM of the Gaussian filter without and with PSF reconstruction is considered appropriate to avoid the positive bias of RC_{max}. Using Gaussian filters less than 4mm for small objects leads to better quantification at the cost of overestimating larger spheres (diameters of 17, 22, and 28mm).

Figure 7 illustrates the effect of reconstruction algorithms with respect to sphere size. The reconstruction sets were selected as 32 sub-iterations with 4mm and 6mm FWHM of Gaussian filters, without and with PSF, respectively. The RC values increased with size, approaching one for spheres larger than 17mm at SBR more than 6.

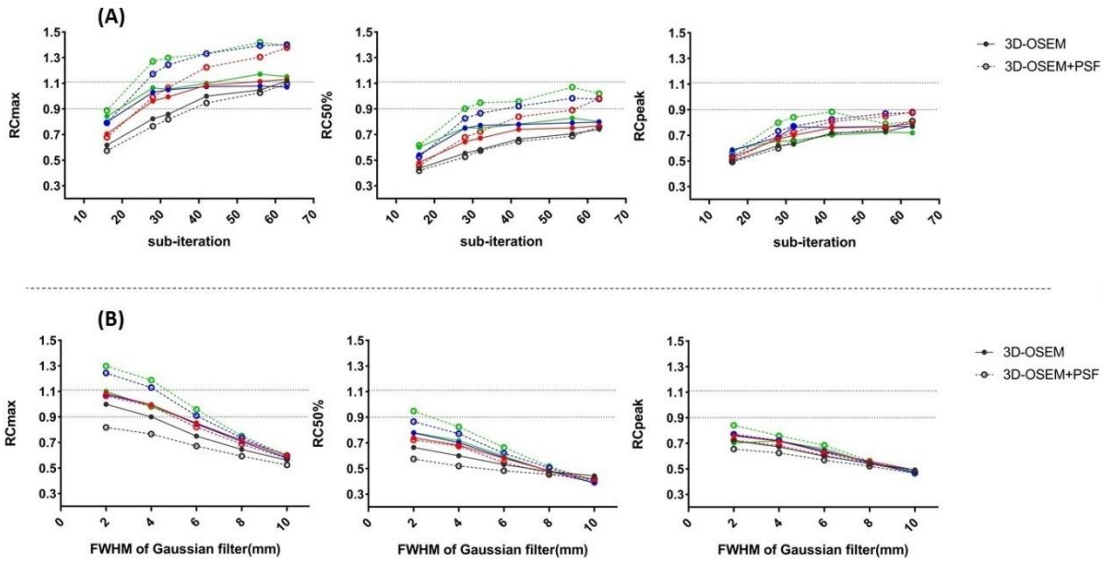

Figure 6. Curves of RC_{max}, $RC_{50\%}$, and RC_{peak} as a function of sub-iteration numbers and FWHM of Gaussian filter in all SBRs. All curves were plotted for a 17mm sphere. RCs against sub-iterations using no smoothing filter (7A), and RCs as a function of Gaussian filter FWHM in constant sub-iteration 32 (7B). (Gray=SBR4, Red=SBR6, Blue=SBR8, Green=SBR10)

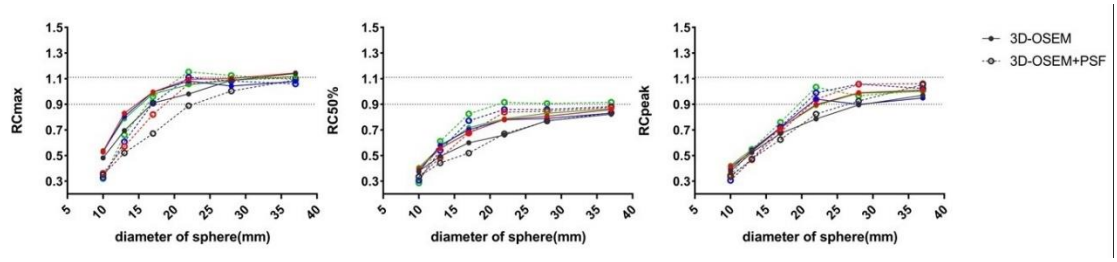

Figure 7. Curves of RC_{max}, $RC_{50\%}$, and RC_{peak} as a function of sphere diameter using sub-iteration 32 with 4 mm/6 mm, without/with PSF reconstruction (Gray=SBR4, Red=SBR6, Blue=SBR8, Green=SBR10)

DISCUSSION

Scan time optimization

PET/CT is a time-consuming examination in clinical practice, and achieving adequate PET image quality is challenging [12]. Due to radiation safety considerations, it is not sufficient to simply increase injected radioactivities to overcome the poor image quality resulting from the short scanning time. Conversely, long acquisition duration without effective positioning may lead to motion artifacts due to patient discomfort and image misalignment [13]. SUV_{max} is most affected by image noise and may especially alter in short acquisition durations [13]. Therefore, optimizing the acquisition duration per bed position can increase the cost-effectiveness of PET imaging. According to the present results, increasing the time per bed position was associated with improved CNR and reduced image noise (CV%). These results are in agreement with a study that compared PET/MRI and PET/CT systems for the assessment of image quality by focusing on detectability [14].

The evaluation of CNR demonstrated that the acquisition duration could be reduced to 60seconds with a slight reduction in lesion detectability. The smallest sphere at SBR 4 could not be visualized when the acquisition duration was less than 60 seconds. The CNR increased from 30 to 60 seconds of scan time, while the image noise was high. However, no significant difference in CV% was found in the acquisition duration of 90 seconds. Therefore, acquisition duration of 90 seconds was recommended to obtain adequate image quality while considering lesion detectability and noise.

Similarly, Brown et al. [15] investigated the impact of acquisition duration on PET image quality. A significant reduction in CV was observed by increasing the acquisition duration to three minutes. Although the image quality only showed minor deterioration between 3 and 4 minutes of acquisition, it dramatically decreased when the acquisition duration was reduced to 2 minutes or less. Our results are in agreement with those reported by Halpern et al. [16], which showed that all lesions could be identified within 3 and 4 minutes of acquisition per bed position, and only four lesions were missed in 1 minute.

The effect of acquisition duration on SUVs is not fully known. According to our phantom experiments, RC_{max} is the most time-dependent parameter. While no significant difference was found in the RC_{max}, $RC_{50\%}$, and RC_{peak} in different acquisition duration. Besides, the low RMSE of RC_{peak} revealed that it is the most accurate quantification parameter. From a clinical point of view, Sher et al. [13] evaluated the impact of scan time on the SUV of healthy livers and tumors acquired on a PET/CT GE Discovery 690 scanner. Fluctuations of SUVs over time were measured within ten minutes (as reference time). However, no significant difference was observed for acquisitions longer than three minutes. This study also concluded that SUV_{peak} had the greatest stability and reproducibility for acquisition duration longer than 1.5 minutes.

Furthermore, in a study by Hausmann et al. [12], although a reduction in acquisition duration from 3 to 1.5 minutes slightly reduced the image quality, no significant difference was observed in the SUV_{max}. Another clinical study on head and neck cancer patients showed a significant decrease in the SUV_{max} variability at acquisition duration longer than three minutes, using a Gemini PET-CT scanner (Philips Co., Cleveland, Ohio, USA) [17]. PET reconstructed images did not show a difference in RCs between acquisition durations. Image quality quantitative indices showed the possibility of lesion detection in the 60 sec scan duration images reconstructed using the routine imaging protocol. In contrast, no differences after 90 sec were found in image noise. Changes in reconstruction parameters could affect the optimized acquisition duration. Nevertheless, the overall perceived image quality was appropriate for all reconstruction settings in acquisition duration more than 180 seconds.

Optimization of reconstruction setup regarding image quality

Based on the findings, the reconstruction parameters strongly influenced image quality and lesion detection. Image noise increased by increasing the number of iterations and reducing the FWHM of the Gaussian filter, as reported in several studies [18-20]. Our results are also in agreement with the results of a study by Machado et al. [21], which showed that using smoother filters or PSF correction reduced the image noise. According to the EARL procedure, CV should remain lower than 15% in PET images [4]; this criterion was relevant for most reconstruction settings in our study. In summary, reconstruction parameter sets, which cause CV above 15%, include many sub-iterations with the lowest FWHM of the Gaussian filter in the non-PSF reconstruction algorithm and in the short acquisition duration.

A study designed to optimize the reconstruction parameters for 90-Y PET/CT imaging demonstrated that the CNR was reduced in more than 42 sub-iterations. Based on the CNR

assessments, fewer iterations (<42) and smoother filters were proposed to achieve higher detectability [20]. In the present study, maximum CNR was observed at fewer sub-iterations (n=16) with smoother filters (FWHM=10mm). Moreover, the contrast was investigated along with CNR due to the discrepancy between CNR and visual assessments. The trade-off between CNR and contrast, especially for the smallest sphere, was determined as the most appropriate reconstruction set to achieve the best image quality and detectability.

An increase in the sub-iteration number with and without reduction in the FWHM of the Gaussian filter resulted in higher contrast, while the image noise increased. This finding is similar to the results of a study by Akamatsu et al. [19], which showed that increasing the sub-iteration number improved the CNR and contrast; it had the greatest impact on contrast in the detectability assessment. A smoother Gaussian filter only improved the CNR with aggravation of contrast. The CNR was less than 5 with 4mm FWHM or less, even when using PSF correction; however, the contrast was the highest with 2mm FWHM. Also, the visual assessment demonstrated that the highest CNR due to using a smoother filter did not guarantee the best image quality. The qualitative and quantitative image quality assessments proposed the optimized reconstruction protocol as 32-63 sub-iterations with 4-6mm FWHM of Gaussian filter, using resolution recovery.

Effects of reconstruction parameters on PET image quantification

For therapy monitoring in multicenter clinical studies, variability in quantitative results should be considered. Harmonization reduces the variability utilizing RCs that mimic SUVs in clinical studies. It should be noted, although harmonization using different RCs has been proposed, their consistency when applied to patient studies has yet to be demonstrated. RC strongly depends on the PET scanner performance, image reconstruction parameters, and accuracy of various corrections during image reconstruction [22]. The reconstruction parameters are known to play an especially critical role. Our phantom experimental setup was useful in standardizing and optimizing the image reconstruction parameters for quantification. We investigated the performance of reconstruction algorithms for the quantitative analysis of PET images in various sphere sizes at varying SBRs.

The results of the present study indicated that the lesion size influenced the RC. When the object was large, the RC value approached one. Overall, the RC was significantly less than one for small objects; these difficulties of PET imaging are attributed to the partial volume effect (PVE) [23]. Although the resolution recovery algorithm provides better spatial resolution and detectability, it causes the overestimation of RC for large sphere sizes in NEMA phantoms (diameter >17 mm). Also, an overshoot along the object's edge (edge artifact) was observed [24].

Our results showed that edge artifacts mostly occur at high SBRs, using high numbers of sub-iterations with lower FWHM of Gaussian filters. These findings confirmed the results of a study by Bai et al. [25], which showed that the overshoot depends on the sphere size and SBR, especially at higher SBRs. Moreover, Tsutsui et al. [26] demonstrated that the size of objects in the non-PSF algorithm was slightly overestimated, and no edge artifact appeared; however, the objects seemed sharp, with edge enhancement using PSF correction. They concluded that PSF modeling caused an edge artifact; the object size, number of iterations, and FWHM of the Gaussian filter were variable and determined its severity.

According to Figure 6, the RCs continued to increase as a function of the sub-iteration number, especially RC_{max}; they continued to reduce by applying more FWHM of the post-smoothing filter. The strong dependence of SUV_{max} on the reconstruction parameters has been reported in several studies [27-29], indicating the highest reproducibility and the least variability of SUV_{peak} [27, 30]. Using a suitable FWHM could eliminate edge artifacts and lead to accurate quantification. Nevertheless, a post-smoothing filter should not be selected too wide, as it would unnecessarily reduce the RC. The EANM guideline stated that the FWHM of spatial post-smoothing filters should not exceed 7mm [4]. In our study, the edge artifact was almost suppressed using 4 to 6 mm FWHM of Gaussian filters. Besides, using peak values instead of maximum values could minimize overestimations.

CONCLUSION

The acquisition duration was more influential on image quality while slightly influencing PET quantitative parameters. It could be reduced without degradation of image quality as assessed by the proposed framework. Consequently, a close agreement between the optimized and standardized setups could lead to developing a reconstruction mode that would provide standardized and consistent quantitative values while maintaining good lesion detectability.

REFERENCES

1. Boellaard R, O'Doherty MJ, Weber WA, Mottaghy FM, Lonsdale MN, Stroobants SG, Oyen WJ, Kotzerke J, Hoekstra OS, Pruim J, Marsden PK, Tatsch K, Hoekstra CJ, Visser EP, Arends B, Verzijlbergen FJ, Zijlstra JM, Comans EF, Lammertsma AA, Paans AM, Willemsen AT, Beyer T, Bockisch A, Schaefer-Prokop C, Delbeke D, Baum RP, Chiti A, Krause BJ. FDG PET and PET/CT: EANM procedure guidelines for tumour PET imaging: version 1.0. Eur J Nucl Med Mol Imaging. 2010 Jan;37(1):181-200.
2. Adams MC, Turkington TG, Wilson JM, Wong TZ. A systematic review of the factors affecting accuracy of SUV measurements. AJR Am J Roentgenol. 2010 Aug;195(2):310-20.
3. Boellaard R. Standards for PET image acquisition and quantitative data analysis. J Nucl Med. 2009 May;50 Suppl 1:11S-20S.
4. Boellaard R, Delgado-Bolton R, Oyen WJ, Giammarile F, Tatsch K, Eschner W, Verzijlbergen FJ, Barrington SF, Pike LC, Weber WA, Stroobants S, Delbeke D, Donohoe KJ, Holbrook S, Graham MM, Testanera G, Hoekstra OS, Zijlstra J, Visser E, Hoekstra CJ, Pruim J, Willemsen A, Arends B, Kotzerke J, Bockisch A, Beyer T, Chiti A, Krause BJ; European Association of Nuclear Medicine (EANM). FDG PET/CT: EANM procedure guidelines for tumour imaging: version 2.0. Eur J Nucl Med Mol Imaging. 2015 Feb;42(2):328-54.
5. Delbeke D, Coleman RE, Guiberteau MJ, Brown ML, Royal HD, Siegel BA, Townsend DW, Berland LL, Parker JA, Hubner K, Stabin MG, Zubal G, Kachelriess M, Cronin V, Holbrook S. Procedure guideline for tumor imaging with 18F-FDG PET/CT 1.0. J Nucl Med. 2006 May;47(5):885-95.
6. Graham MM, Wahl RL, Hoffman JM, Yap JT, Sunderland JJ, Boellaard R, Perlman ES, Kinahan PE, Christian PE, Hoekstra OS, Dorfman GS. Summary of the UPICT protocol for 18F-FDG PET/CT imaging in oncology clinical trials. J Nucl Med. 2015 Jun;56(6):955-61.
7. Ferretti A, Chondrogiannis S, Rampin L, Bellan E, Marzola MC, Grassetto G, Gusella S, Maffione AM, Gava M, Rubello D. How to harmonize SUVs obtained by hybrid PET/CT scanners with and without point spread function correction. Phys Med Biol. 2018 Nov 26;63(23):235010.
8. Kaalep A, Sera T, Rijnsdorp S, Yaqub M, Talsma A, Lodge MA, Boellaard R. Feasibility of state of the art PET/CT systems performance harmonisation. Eur J Nucl Med Mol Imaging. 2018 Jul;45(8):1344-61.
9. Vosoughi H, Hajizadeh M, Emami F, Momennezhad M, Geramifar P. PET NEMA IQ Phantom dataset: image reconstruction settings for quantitative PET imaging. Data Brief. 2021 Jun 18;37:107231.
10. Vosoughi H, Momennezhad M, Emami F, Hajizadeh M, Rahmim A, Geramifar P. Multicenter quantitative ^{18}F-fluorodeoxyglucose positron emission tomography performance harmonization: use of hottest voxels towards more robust quantification. Quant Imaging Med Surg. 2023 Apr 1;13(4):2218-33.
11. Lammertsma AA, Boellaard R. The need for quantitative PET in multicentre studies. Clin Transl Imaging. 2014;2(4):277-80.
12. Hausmann D, Dinter DJ, Sadick M, Brade J, Schoenberg SO, Büsing K. The impact of acquisition time on image quality in whole-body 18F-FDG PET/CT for cancer staging. J Nucl Med Technol. 2012 Dec;40(4):255-8.
13. Sher A, Lacoeuille F, Fosse P, Vervueren L, Cahouet-Vannier A, Dabli D, Bouchet F, Couturier O. For avid glucose tumors, the SUV peak is the most reliable parameter for [18 F] FDG-PET/CT quantification, regardless of acquisition time. EJNMMI res. 2016;6(1):21.
14. Øen SK, Aasheim LB, Eikenes L, Karlberg AM. Image quality and detectability in Siemens Biograph PET/MRI and PET/CT systems-a phantom study. EJNMMI Phys. 2019 Aug 5;6(1):16.
15. Brown C, Dempsey MF, Gillen G, Elliott AT. Investigation of 18F-FDG 3D mode PET image quality versus acquisition time. Nucl Med Commun. 2010 Mar;31(3):254-9.
16. Halpern BS, Dahlbom M, Quon A, Schiepers C, Waldherr C, Silverman DH, Ratib O, Czernin J. Impact of patient weight and emission scan duration on PET/CT image quality and lesion detectability. J Nucl Med. 2004 May;45(5):797-801.
17. Goethals I, D'Asseler Y, Dobbeleir A, Deblaere K, Ham H. The effect of acquisition time on visual and semi-quantitative analysis of F-18 FDG-PET studies in patients with head and neck cancer. Nucl Med Commun. 2010 Mar;31(3):227-31.
18. Prieto E, Martí-Climent JM, Morán V, Sancho L, Barbés B, Arbizu J, Richter JA. Brain PET imaging optimization with time of flight and point spread function modelling. Phys Med. 2015 Dec;31(8):948-55.
19. Akamatsu G, Ishikawa K, Mitsumoto K, Taniguchi T, Ohya N, Baba S, Abe K, Sasaki M. Improvement in PET/CT image quality with a combination of point-spread function and time-of-flight in relation to reconstruction parameters. J Nucl Med. 2012 Nov;53(11):1716-22.
20. Khazaee M, Kamali-Asl A, Geramifar P, Rahmim A. Low-dose 90Y PET/CT imaging optimized for lesion detectability and quantitative accuracy: a phantom study to assess the feasibility of pretherapy imaging to plan the therapeutic dose. Nucl Med Commun. 2017 Nov;38(11):985-97.
21. Machado MAD, Menezes VO, Namías M, Vieira NS, Queiroz CC, Matheoud R, Alessio AM, Oliveira ML. Protocols for Harmonized Quantification and Noise Reduction in Low-Dose Oncologic ^{18}F-FDG PET/CT Imaging. J Nucl Med Technol. 2019 Mar;47(1):47-54.
22. Kelly MD, Declerck JM. SUVref: reducing reconstruction-dependent variation in PET SUV. EJNMMI Res. 2011 Aug 18;1(1):16.
23. Munk OL, Tolbod LP, Hansen SB, Bogsrud TV. Point-spread function reconstructed PET images of sub-centimeter lesions are not quantitative. EJNMMI Phys. 2017 Dec;4(1):5.
24. Rahmim A, Qi J, Sossi V. Resolution modeling in PET imaging: theory, practice, benefits, and pitfalls. Med Phys. 2013 Jun;40(6):064301.
25. Bai B, Esser PD. The effect of edge artifacts on quantification of positron emission tomography. IEEE Nucl Sci Symp Med Imaging Conf. 2010:2263-6.
26. Tsutsui Y, Awamoto S, Himuro K, Umezu Y, Baba S, Sasaki M. Edge artifacts in point spread function-based PET reconstruction in relation to object size and reconstruction parameters. Asia Ocean J Nucl Med Biol. 2017 Spring;5(2):134-43.
27. Sheikhbahaei S, Marcus C, Wray R, Rahmim A, Lodge MA, Subramaniam RM. Impact of point spread function reconstruction on quantitative 18F-FDG-PET/CT imaging parameters and inter-reader reproducibility in solid tumors. Nucl Med Commun. 2016 Mar;37(3):288-96.
28. Bettinardi V, Castiglioni I, De Bernardi E, Gilardi M. PET quantification: strategies for partial volume correction. Clin Transl Imaging. 2014;2(3):199-218.
29. Prieto E, Domínguez-Prado I, García-Velloso MJ, Peñuelas I, Richter JÁ, Martí-Climent JM. Impact of time-of-flight and point-spread-function in SUV quantification for oncological PET. Clin Nucl Med. 2013 Feb;38(2):103-9.
30. Devriese J, Beels L, Maes A, Van de Wiele C, Pottel H. Impact of PET reconstruction protocols on quantification of lesions that fulfil the PERCIST lesion inclusion criteria. EJNMMI Phys. 2018 Dec 7;5(1):35.